

RESEARCH

Received 12 May 2025 Accepted 30 July 2025 Available online 5 August 2025 Version of Record published 5 September 2025

OXYSTEROLS AND PHYTOSTEROLS IN HUMAN PATHOPHYSIOLOGY

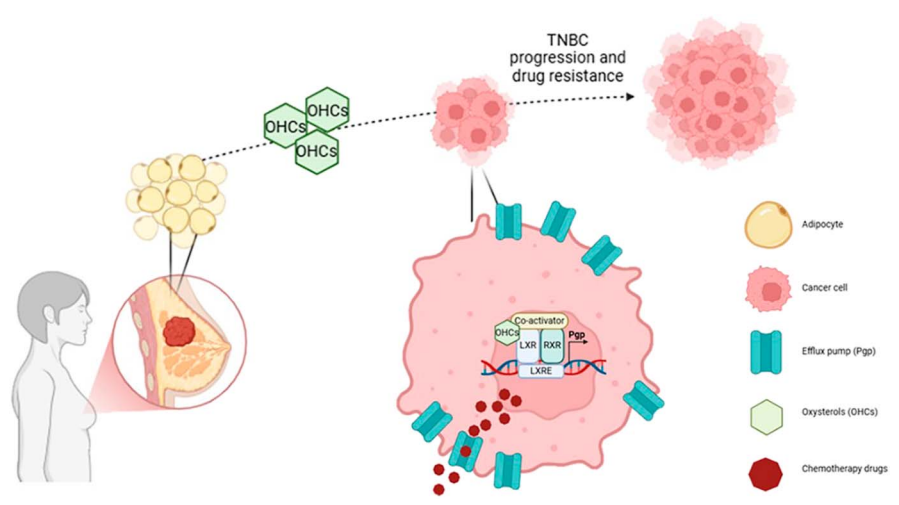
Adipocytes in tumour microenvironment promote chemoresistance in triple-negative breast cancer through oxysterols

Alex Websdale¹, Yusur Al-Hilali², Baek Kim³, Bethany J Williams^{4,5}, Laura Wastall⁴, Hanne Roberg-Larsen^{6,7}, Thomas A Hughes[©]^{2,8}, Giorgia Cioccoloni[©]¹ and James L Thorne[©]¹

Correspondence should be addressed to G Cioccoloni: g.cioccoloni@leeds.ac.uk or to J L Thorne: j.l.thorne@leeds.ac.uk

This article forms part of the Oxysterols and Phytosterols in Human Pathophysiology special collection.

Graphical abstract



Adipocytes-derived oxysterols protect TNBC cells from chemotherapy activating LXR α -Pgp axis. Figure generated with Biorender.



¹School of Food Science & Nutrition, University of Leeds, Leeds, United Kingdom

²School of Medicine, University of Leeds, Leeds, United Kingdom

³Department of Breast Surgery, St. James's University Hospital, Leeds, United Kingdom

⁴Department of Histopathology, Leeds Teaching Hospitals NHS Trust, Leeds, United Kingdom

⁵Department of Pathology, University of Leeds, Leeds, United Kingdom

⁶Section for Chemical Life Sciences, Department of Chemistry, University of Oslo, Oslo, Norway

⁷Hybrid Technology Hub - Centre of Excellence, Institute of Basic Medical Sciences, Faculty of Medicine, University of Oslo, Oslo, Norway

⁸School of Science, Technology and Health, York St John University, York, United Kingdom

Abstract

Objective: Triple-negative breast cancer (TNBC) patients with excess adipose tissue experience poorer disease-free survival than those with a healthy body mass index. Adipocytes store and release cholesterol, which can be hydroxylated to form oxysterols. These cholesterol derivatives activate the liver X receptor (LXR) pathway. This study tested the hypothesis that adipocytes contribute to an imbalanced tumour microenvironment by exposing cancer cells to elevated oxysterols, mimicking chemotherapy exposure conditions and priming for chemoresistance.

Methods: Tumour tissue microarray from 148 TNBC patients was assessed using immunohistochemistry for CH25H, CYP46A1, CYP27A1, P-glycoprotein (Pgp/ABCB1) expression and survival outcomes were assessed. Gene expression was compared between tumours from patients (GSE78958) and mouse models (GSE151866) with high versus low adiposity. In vitro, cell lines from lineages found in the tumour microenvironment were evaluated for oxysterol content, secretion, expression of relevant enzymes, and ability to induce ABCB1 expression and drug resistance in TNBC cells.

Results: In patients, stromal expression of oxysterol-synthesising enzymes correlated with ABCP1 expression in cancer epithelial cells and was associated with shorter disease-free survival. Adipocytes-conditioned media contained significantly higher oxysterol levels than that conditioned by other cell types and induced ABCB1 expression and drug resistance in MDA.MB.468 cells. Obese mice had elevated levels of *Abcb1* in tumours compared to lean counterparts.

Conclusion: Adipocytes secrete oxysterols that promote drug resistance *in vitro* and correlate with oxysterol: Pgp axis and survival *in vivo*.

Significance statement

This study reveals a mechanism by which adipose tissue contributes to drug resistance in ER-negative breast cancers, identifying the oxysterol–Pgp axis as a potential therapeutic target.

Keywords: triple-negative breast cancer; drug resistance; adipose tissue; oxysterols

Introduction

Triple-negative breast cancer (TNBC) is a subtype of breast cancer defined by the lack of expression of oestrogen, progesterone and HER2 receptors. The absence of these receptors, which, when expressed in other subtypes, can be targeted with systemic hormone therapy or anti-HER2 therapy, means that these cancers can only be systemically treated with cytotoxic chemotherapy and, in some cases, immunotherapy (Schmid et al. 2018, Schmid et al. 2020). TNBC drug resistance is a significant challenge, and disease relapse can occur rapidly (Dent et al. 2007). The mechanisms of drug resistance in TNBC are complex and, given disease heterogeneity, remain poorly understood. Overweight TNBC patients treated with chemotherapy have shorter disease-free survival (DFS) and overall survival compared to lean patients (Harborg et al. 2021), suggesting an interaction between adipose tissue and systemic chemotherapy.

TNBC is a category of exclusion and is defined when the tumour lacks expression of three theranostic targets, namely: oestrogen receptor (ER), progesterone receptor and human epidermal growth factor receptor (HER2).

Although novel targeted therapies pembrolizumab (PDL1 inhibitor) and talazoparib (PARPi) are emerging, standard treatment options remain limited to surgery, radiotherapy and, owing to lack of therapeutic target expression, systemic cytotoxic chemotherapy. This cancer of unmet clinical need relapses frequently (20–50% relapse within 5 years) and rapidly (median 2.6 years), indicating failure of systemic chemotherapy to fully eradicate residual tumour cells (Liedtke et al. 2008). Multiple mechanisms of chemoresistance have been proposed for TNBC, including dysregulated cholesterol homeostasis. The LXR-Pgp pathway, driven by oxysterols, was previously reported to be associated with poor outcomes for TNBC patients treated with chemotherapy. Pgp, a membrane-bound drug efflux pump, can export many of the chemotherapy agents used in the systemic treatment of TNBC patients (Hutchinson et al. 2021).

The extensive heterogeneity of the TNBC microenvironment (TME) and the tumour's mutational profiles make predicting which patients will suffer with drug resistance challenging. A high stroma-to-tumour

ratio is associated with worse DFS, particularly for TNBC patients (Kramer et al. 2019, Millar et al. 2020). The TME typically consists of immune cells and stromal cells such as fibroblasts, which mount a cytoprotective interferon-b response to chemotherapy exposure (Millar et al. 2020, Broad et al. 2021). Adipocytes also comprise a significant proportion of the breast cancer TME. Adipose tissue contains up to 25% of the body's total cholesterol. rising to as much as 50% in obese individuals (Krause & Hartman 1984). For this reason, overweight and obese patients' breast tumours are particularly highly exposed to adipocyte cholesterol stores (Krause & Hartman 1984). Circulating cholesterol is typically found in dynamic equilibrium with adipose cholesterol stores, and elevated cholesterol levels at diagnosis are associated with lower DFS (Rodrigues dos Santos et al. 2014), in a manner that cholesterol metabolism should be considered as a therapeutic target alongside chemotherapy.

Oxysterols are endogenous liver x receptor alpha (LXRa) ligands (Janowski et al. 1996, Janowski et al. 1999), which are derived from cholesterol by a single enzymatic hydroxylation reaction on cholesterol's side chain; their further metabolism leads to production of bile acids, seco-steroids, steroid hormones and other important endocrine or paracrine factors (Slenter et al. 2018). Oxysterols are found in breast cancer-secreted exosomes (Roberg-Larsen et al. 2017) and in both ER-negative and ER-positive primary breast tumours at concentrations that activate LXR signalling (Solheim et al. 2019). ER-negative breast cancers are significantly more responsive to oxysterol signalling compared to other subtypes (Hutchinson et al. 2019), and in TNBC, expression of LXRa splice variants that lack the oxysterol-binding domain is associated with longer DFS in TNBC (Lianto et al. 2021). Oxysterol-driven LXRa activity induces expression and function of the P-glycoprotein (Pgp) efflux pump and is associated with chemoresistance in TNBC patients (Hutchinson et al. 2021). However, the association between circulating oxysterols and breast cancer-specific outcomes still produces conflicting results (Decker et al. 2023). Here, we have tested the hypothesis that the proximity and integration of adipose tissue mean that the TNBC microenvironment is exposed to elevated levels of oxysterols, which confer chemotherapy resistance in TNBC via Pgp.

Methods

Cell lines

All cell lines were routinely maintained at 37°C with 5% CO2 and tested for mycoplasma every 6 months. TNBC cell lines MDA.MB.468 and MDA.MB.453 were obtained from ATCC and were routinely passaged in Dulbecco's Modified Eagle Medium (DMEM) GlutaMAX

(DMEM, Thermo Fisher, UK, Cat: 31966047) and supplemented with 10% FCS (Thermo Fisher, UK, Cat: 11560636), or when indicated for oxysterol pellet analysis, were instead cultured in CHUB-S7 media (see below). Generation and application (Hutchinson et al. 2019) of MDA.MB.468 LXRa luciferase reporter cells has been described previously. Human pre-adipocyte CHUB-S7 stem cells, donated by Nestlé Research Centre, were originally isolated from subcutaneous abdominal adipose tissue of a 33-year-old obese female patient and immortalised by overexpressing hTERT as previously described (Darimont et al. 2003). CHUB-S7 were maintained in DMEM/Nutrient F12 Hams, supplemented with 10% FCS and 2 mM glutamine (Sigma, UK, Cat; G7513). CHUB-S7s were differentiated into mature adipocytes (mAdipo) as previously described (Darimont et al. 2006), using differentiation medium supplemented with rosiglitazone (Cayman Chemical, USA, Cat: 71740) and 100 U/mL penicillin/streptomycin (Sigma, UK, Cat: P0781). Cancer-associated fibroblast (CAF) cell line was generated by viral-mediated immortalisation through overexpression of hTERT in fibroblasts extracted from breast tumours as previously described (Broad et al. 2021) and routinely passaged in Dulbecco's Modified Eagle Medium (DMEM) GlutaMAX (DMEM, Thermo Fisher, UK, Cat: 31966047) and supplemented with 10% FCS (Thermo Fisher, UK, Cat: 11560636).

Drugs and reagents

Epirubicin (Cayman, USA, Cat: 12091) was diluted in nuclease-free water and protected from light. 24S-hvdroxycholesterol (24OHC), 25-hvdroxycholesterol (250HC) and 27-hydroxycholesterol (270HC, also known as 26-hydroxycholesterol and 25R26-hydroxycholesterol), together with internal standards (25-hydroxycholesterold6 and 27-hydroxycholesterol-d6), were from Avanti Polar Lipids (USA). Stock solutions and calibration solutions were prepared as described in Solheim et al. (2019). TagMan assays (Thermo Fisher, UK, Cat: 4331182): Pgp/ABCB1 (Hs00184500 m1), ABCA1 (Hs01059137 m1), CYP27A1 (Hs0016803_m1), CYP46A1 (Hs1042347_m1), CH25H (Hs04187516 m1) and HPRT1 (Hs02800695 m1). All stocks were stored at -20° C. Antibodies used for IHC were: Pgp (Santa Cruz Biotech, USA, Cat: sc73354), CYP27A1 (Abcam, UK - Cat: ab126785), CYP46A1 (Abcam, UK - Cat: ab198889), CH25H (Bioss, USA - Cat: bs6480R) and were validated previously as described (Hutchinson et al. 2021).

Conditioning of culture media by adipocytes and cancer-associated fibroblasts

Mature adipocyte-conditioned media (mAdipo-CM) was generated by adding 15 mL of DMEM/F12 with 10% charcoal-stripped FBS (CS-FBS) into a confluent T75 and incubating for $48\ h.$

MDA.MB.468 CM (vehicle) was generated by seeding 4.5 \times 10⁶ cells/mL into a T75, adding 15 mL of DMEM/F12 containing CS-FBS, and incubating for 48 h. CM was centrifuged upon collection for 5 min at 200 g and used fresh or stored at -80° C until use.

Once CM was collected, 6×10^5 cells/well of MDA.MB.468 cells were seeded in 6-well plates and exposed to vehicle or mAdipo-CM for 16 h, 24 and 48 h. At the end of each treatment, cells were suspended in different buffers to be assessed for luciferase expression, MTT or mRNA expression.

CAF-CM was generated by adding 10 mL of DMEM containing 10% FBS into a confluent T75 and incubating for 44 h. To match CAF-CM pH, MDA.MB.468 CM was generated by seeding 4.5×10^5 cells/mL and conditioning DMEM containing 10% FBS for 24 h. All media were centrifuged upon collection for 5 min at 200 g and stored at -80° C until use.

Cell viability assay

For the cell proliferation assay, MDA.MB.468 cells were treated with vehicle or mAdipo-CM as previously described. Cells were then trypsinised, washed and suspended in 200 µL of PBS, and distributed into a 96-well plate (90 μ L/well). For the cell drug resistance assay, 2×10^4 /well MDA.MB.468 cells were seeded in a 96-well plate for 4 h and then treated with either vehicle CM or mAdipo-CM to reach the volume of 200 µL/well for 24 or 48 h, respectively. For the chemoresistance assay, epirubicin (Cayman Chemical, USA, Cat: 12091) was then added at different concentrations for 48 h. Cells were washed, and MTT reagent was added at a final concentration of 0.5 mg/mL. In all experiments, after 4 h incubation at 37°C, the MTT solution was removed and replaced with 100 µL of DMSO/well. Absorbance at 540 nm was read using a CLARIOstar Plus microplate reader.

Luciferase assay

Luciferase assays were performed by pelleting 100 μL of MDA.MB.468 cells and suspending them in 100 μL of Reporter Lysis Buffer (Promega, UK, Cat: E1500). 20 μL of cell lysate was distributed into white-walled 96-well plates, and luciferase expression was measured using the Luciferase Assay System (Promega, UK, Cat: E1500) through luminescent signal using the CLARIOstar Plus microplate reader (BMG LABTECH, Germany). Results were subsequently normalised using cell proliferation data to eliminate the proliferative effect of mAdipo-CM on TNBC cells, which could have distorted the luciferase data.

Analysis of gene expression

Analysis of gene expression was performed as described previously (Hutchinson *et al.* 2019). Briefly, ReliaPrep

Minipreps for cell cultures (Promega, UK, Cat: Z6012) was used to extract mRNA, and GoScriptTM (Promega, UK, Cat: A5003) was used for cDNA synthesis. TaqMan Fast Advanced Master Mix (Thermo Fisher, UK, Cat: 4444557) was mixed with TaqMan assays and analysed in the QuantStudio Flex 7 (Applied Biosystems Life Tech, Thermo Scientific, UK).

Immunohistochemistry and adipocyte scoring

IHC was performed as previously described (Hutchinson et al. 2021). Tissue microarray (TMA) block sections were dewaxed in xylene and dehydrated in ethanol. For Pgp, CYP46A1 and CH25H antibodies, antigen retrieval was not performed. For the CYP27A1 antibody, slides were heated in citrate buffer. Endogenous peroxidase activity was blocked with 0.3% H₂O₂ in methanol, and for Pgp, CYP46A1 and CH25H, a further blocking step was carried out using BlockerTM Casein in TBS (37532, Thermo Fisher Scientific, UK). Slides were incubated with antibodies for 1 h. Staining was visualised using secondary antibodies and the SignalStain DAB substrate kit (Cell Signalling Technology, NL, Cat: 80595). Nuclei were stained with Mayer's haematoxylin and washed with Scott's tap water. Sections were dehydrated with ethanol, washed with xylene and mounted onto coverslips with DePeX Fluka. Immunohistochemical staining within stromal regions was quantified using the Positive Pixel Count version 9 algorithm (Aperio Technologies, USA) for ImageScope. Briefly, positive staining of Pgp, CYP27A1, CH25H and CYP46A1 was assessed semi-quantitatively using a weighted histoscore system. Each tumour was scored in triplicate, with three cores embedded per tumour. Histoscores between 0 and 300 were determined, with this value calculated using the formula: $(1 \times \%)$ of tumour cells weakly stained) + $(2 \times \%)$ of tumour cells moderately stained) + $(3 \times \%)$ of tumour cells strongly stained). Weighted histoscores were calculated for total stroma of the three enzymes and Pgp. Tumours were ignored if two or more duplicate cores were missing. For scoring of TMA sections, whole cores were scored. Accuracy of primary observer histoscores was previously reported (Hutchinson et al. 2021).

Stromal proportions of tumour cores were measured using ImageScope version 12.4.3 (Aperio Technologies, USA) by drawing around the perimeter of the core, excluding necrotic regions, and drawing around cancer regions in the core. Cancer area was then subtracted from the total area to find the stromal area of the core. Stromal area was then divided by total area to find the stromal proportion of the tumour.

Adipocyte count was performed on each tumour and scored in triplicate, with three cores embedded per tumour. Tumours were ignored if two or more replicate cores were missing. Accuracy of the primary observer was verified by an independent observer for

all tumour cores. Intraclass correlation was based on McGraw & Wong (1996) and the Shrout & Fleiss (1979) convention, and calculated using the two-way mixed-effects, consistency and single-rater method. Presence of adipocytes in each tumour was classified as 0 if none of the cores for that tumour showed adipocytes, or ≥ 1 if at least one core for each tumour showed adipocytes.

Human samples: ethical approval, collection and processing

Ethical approvals were obtained from Leeds (East) REC (reference numbers: 06/Q1206/180, 09/H1306/108). The patient cohort and clinicopathological features have been described previously (Hutchinson et al. 2021) and updated for adipocyte count (Supplementary Table 1. See section on Supplementary materials given at the end of the article). Briefly, selection criteria were: patients with TNBC/basal-like tumours who had not undergone neoadjuvant therapy, tumours with sufficient stroma, absence of heavily necrotic or inflammatory regions, and availability of resection blocks for normal tissue. Haematoxylin/eosin stain was used to identify suitable areas for inclusion in the tissue microarray (TMA). Tumour cores of 0.6 mm were taken in triplicate from 148 tumour samples and transferred into recipient wax blocks.

Oxysterol quantification

MDA.MB.468, MDA.MB.453, CHUB-S7 pre-adipocyte, mature adipocyte and CAF pellets (3 \times 10⁵ cells) were prepared as previously described (Roberg-Larsen et al. 2014), with some modifications. Cell pellets were added to 100 µL of 1.5 nM internal standard solution of deuterated 240HC, 250HC and 260HC (Avanti Polar Lipids, USA) in 2-propanol and shaken well before evaporation to dryness using a speedvac. The pellets were then re-dissolved in 20 µL 2-propanol before derivatisation with Girard T reagent. Cell culture media samples (200 μ L) were prepared as previously described (Kømurcu et al. 2023), with some modifications: aliquots of 100 or 200 μL were mixed with 100 μL of 1.5 nM internal standard solution of deuterated 240HC, 250HC and 260HC (Avanti Polar Lipids, USA) in 2-propanol and shaken well before evaporation to dryness using a speedvac. The residues were re-dissolved in 20 µL isopropanol before derivatisation with Girard T reagent. All samples had a final internal standard concentration of 200 pM and were stored at 4°C before analysis.

All cell and medium samples were analysed within a week using Dionex Ultimate 3000 UHPLC coupled to a TSQ Vantage triple quadrupole mass spectrometer

(Thermo Scientific), as previously described (Solheim et al. 2019). Removal of excess derivatisation reagents and other particulate matter (sample clean-up) was performed on-line using an automatic filtration and filter back-flush (AFFL) solid-phase extraction system.

Analysis of publicly available datasets

Publicly deposited data were obtained to compare TNBC tumours between obese and lean mice (Bousquenaud & Rüegg 2022) (GSE151866) and patients (Toro *et al.* 2016) (GSE78958); details of experimental procedures are available in the corresponding citations. From the mouse dataset, we extracted gene expression data for lean (n = 4) and obese (n = 4) mice. For human samples, we extracted gene expression data and clinical information to select patients with basal-like breast cancer (n = 98) and then classified them by body mass index (BMI) as normal-weight (BMI <25: n = 30), overweight (BMI 25–29.99: n = 34), or obese (BMI ≥ 30 : n = 34).

Statistical analysis

For human cohorts and animal data analysis, a normality test was conducted before subsequent analysis. Analysis of protein correlations was assessed using Spearman rank. Kaplan-Meier analysis with 95% confidence intervals was used for survival curves, and a log-rank test was performed to assess significance. One-way ANOVA with multiple comparisons was used to compare oxysterol content and RNA expression of oxysterol-synthesising enzymes between mAdipo, CAF and breast cancer cell pellets, and between mAdipo-CM, CAF-CM and breast cancer cell CM. One-way ANOVA with multiple comparisons testing was also used to compare LXR transactivation and gene expression. TMA samples containing adipocytes were compared with samples without adipocytes using an unpaired parametric one-tailed *t*-test. Spearman correlation was used to observe associations between gene expression and the different BMI groups from GSE78958. A one-tailed unpaired t-test was used to compare gene expression between lean and obese mice from GSE151866 and MDA.MB.468 gene expression following pre-treatment with mAdipo-CM. A one-tailed paired t-test was used to analyse MTT assay of epirubicin dose response following pre-treatment of MDA.MB.468 with mAdipo-CM. A one-tailed t-test was used because our hypothesis, informed by prior analysis, specifically predicted the direction of the effect, and differences in the opposite direction were not of theoretical interest.

Results

Protein level of oxysterol-synthesising enzymes in non-cancer compartment of the tumour microenvironment is associated with Pgp protein expression in cancer cells and with disease-free survival

To determine whether expression of stromal oxysterol enzymes was associated with Pgp expression in primary TNBC tumours and DFS of patients, we analysed 148 TNBC tumour cores using a tissue microarray (TMA), details of which have been reported previously (Hutchinson et al. 2021). The proportion of the tumour found to be stromal correlated weakly, but significantly, with epithelial expression of Pgp protein ($R^2 = 0.09$; P = 0.0007) (Fig. 1A, right panel). When patients were dichotomised into having high or low stroma-epithelial ratios using receiver operating characteristic (ROC) curves (shown in SF1), a high stroma-to-cancer-cell ratio was, as expected, associated with shorter DFS (P = 0.017) (Fig. 1A). Next, protein levels of the enzymes that convert cholesterol into 24OHC (CYP46A1), 25OHC (CH25H), or 27OHC (CYP27A1) were measured in the non-cancer cell fraction of the tumour (Fig. 1B, C, D). Non-cancer cell expression of all three enzymes was positively correlated with cancer cell expression of Pgp (CYP46A1: $R^2 = 0.22$, P < 0.0001; CH25H: $R^2 = 0.35$, P < 0.0001; CYP27A1: $R^2 = 0.07$, P = 0.0072). Elevated protein expression was associated with significantly shorter DFS for CYP46A1 (P = 0.0075), CH25H (P = 0.0024) and CYP27A1 (P = 0.0183). These correlations and survival curves are consistent with the hypothesis that chemoresistance in TNBC cancer cells could, at least in part, be driven by oxysterols synthesised and secreted by the tumour microenvironment.

Oxysterol synthesis and export by cells of the tumour microenvironment is dominated by adipocytes

The TME comprises a mixture of tumour cells and nontumour 'host' cells. To establish if the tumour's oxysterol pool, and therefore LXR activity within the cancer cell compartment, could be shaped by the non-cancer compartment of the TME, we compared the ability of TNBC cell lines, CAFs (Verghese et al. 2013) and adipocyte cell lines to synthesise and secrete oxysterols, and their ability to activate LXR in cancer cells. First, we measured mRNA expression of the enzymes that synthesise the OHCs previously reported to be present in primary breast tumour samples (Solheim et al. 2019). Synthesis of CYP46A1, the 24OHC-synthesising enzyme, was significantly higher in mAdipo cells than all other cell types (Fig. 2A; P < 0.0001 for all). For CH25H, which generates 250HC, expression was also higher in mAdipo than CAFs, MDA.MB.453 and MDA.MB.468 cell

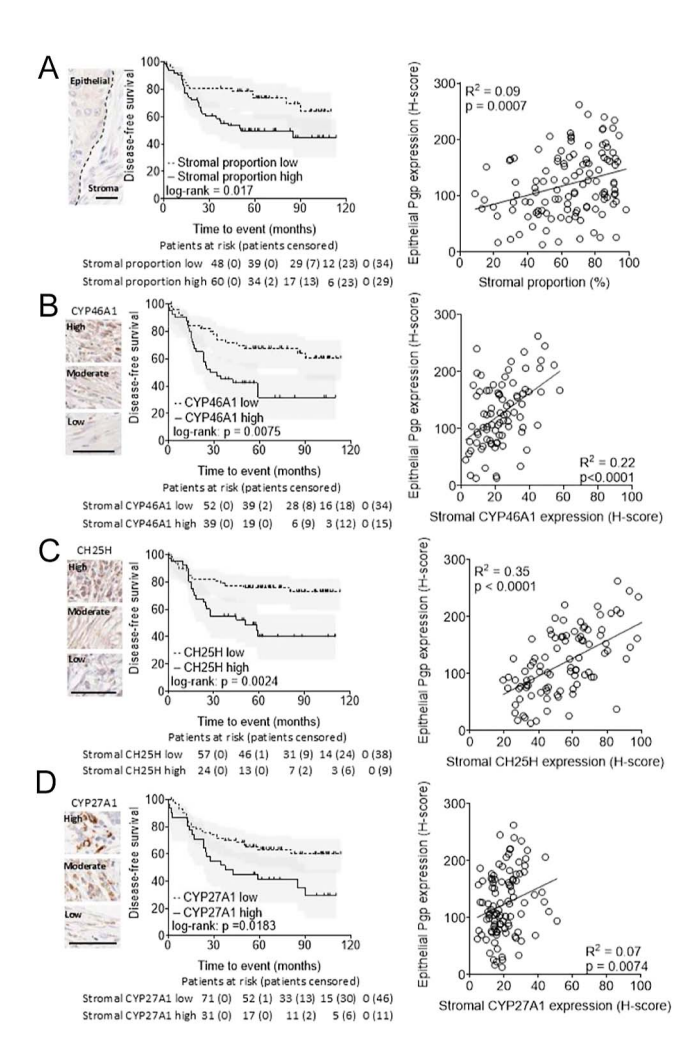


Figure 1

Expression of stromal proportion and relative oxysterol synthesis enzymes in the TNBC microenvironment is associated with elevated Pgp expression and shorter DFS. From left to right, shown are representative images of tumour sections with 25 mm scale bars (left), Kaplan–Meier survival curves (middle), and correlation analysis with cancer epithelial Pgp expression (right). Analyses shown are for epithelial to stromal proportions (A), CYP46A1 (B), CH25H (C) and CYP27A1 (D). Kaplan–Meier is shown with 95% confidence intervals, with log-rank test. Patients at risk of suffering an event are shown beneath. Two-tailed Spearman's rank was used to assess correlation.

lines (Fig. 2B; P=0.0568, P=0.0863, P=0.0721, respectively). Expression of *CYP27A1* was similar between mAdipo and CAFs (Fig. 2C; P>0.05), but both had significantly more mRNA than the TNBC cell lines (P<0.001 for all). Regarding intracellular OHC concentrations, mAdipo had significantly higher levels than the TNBC cell lines for all three OHCs (Fig. 2D, E, F; P<0.05 for all), while CAFs had significantly less 24OHC than mAdipo (P=0.0035) and were statistically equivocal to the TNBC cell lines for 25OHC and 27OHC. To establish if oxysterols were secreted into the TME by the four cell

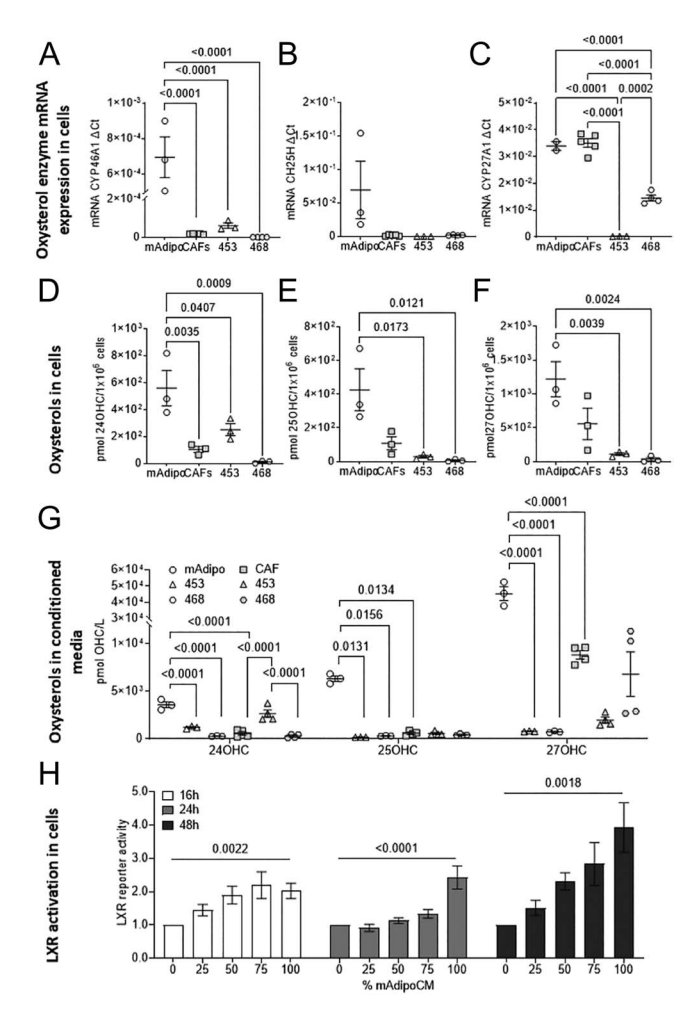


Figure 2

Mature adipocytes but not CAFs contain and secrete higher concentrations of oxysterols relative to cancer epithelial cells. mRNA expression of CYP46A1 (A), CH25H (B) and CYP27A1 (C) from mAdip, CAFs, MDA.MB.468 and MDA.MB.453 cells. Oxysterol concentrations in pellets of 1×10^6 cells (D, E, F). Data shown are mean with SEM of 2–4 independent replicates and are analysed with one-way ANOVA. Media concentrations of 24OHC, 25OHC and 27OHC (G) after conditioning with mAdipo, CAFs, MDA, MB, 468 and MDA, MB, 453 cells, Cancer cell data are shown twice to match the different growth culture media required for mAdipo cells (charcoal stripped DMEM/F12) and CAFs (10% FBS DMEM). Data shown are mean with SEM of 3-4 independent replicates with standard error and are analysed with one-way ANOVA. Conditioned media from mAdipo drives LXR activity in MDA.MB.468 reporter cells (H). Data are normalised using cell proliferation and subsequently normalised to match 0% conditioned media. Data shown are mean with SEM of 7-9 independent replicates and are analysed with one-way ANOVA.

types, we sampled cell culture media after conditioning for 48 h. 270HC was the most abundant oxysterol released into the media by an order of magnitude in mAdipo and CAFs (Fig. 2G). mAdipo-conditioned media contained significantly more OHC compared to CAFs, for

24OHC (7.8-fold, P < 0.0001), 25OHC (11-fold, P = 0.0134) and 27OHC (5.3-fold, *P* < 0.0001) (Fig. 2G). CAF-conditioned media had significantly less OHCs than mAdipo and contained either the same or fewer OHCs than MDA.MB.453 and MDA.MB.468 conditioned media. Finally, to establish if the conditioned media contained sufficient oxysterols to activate LXR signalling in TNBC epithelial cells, we cultured LXR reporter MDA.MB.468 cells in conditioned media. A modest but significant 2.4-fold increase in LXR reporter gene activity was observed after 24 h culture with 100% mAdipo-CM (P < 0.0001). At 48 h, LXR reporter gene activity was induced in a manner dependent on the dose of conditioned media (75% mAdipo-CM: 2.8-fold; 100% mAdipo-CM: 3.9-fold; P = 0.0018) (Fig. 2H). From these data, we concluded that, of the TME components we could utilise in vitro, mAdipo produce significantly higher levels of oxysterols than other cell types.

Adiposity is associated with higher Pgp and CH25H expression in primary tumours

We next hypothesised that if adipocytes could secrete oxysterols, then adipocyte numbers should be associated with enhanced expression of LXR target genes. As we had already measured expression of the LXR target gene ABCB1/Pgp in the TMA cohort (Fig. 1A), we reinterrogated these tumour cores by scoring them for the number of adipocytes present. In tumour cases where there was at least one visible adipocyte, Pgp expression was significantly higher (P = 0.0388) compared to cores where no adipocytes were visible (Fig. 3A). We also found that there were significantly higher levels of another LXR target gene, the 25OHC-synthesising enzyme CH25H (P = 0.039) in cores with at least one adipocyte (SFig. 2A) Supplementary materials). Expression of other OHCsynthesising enzymes CYP46A1 (SFig. 2B) and CYP27A1 (SFig. 2C) in cancer cells was not significantly different between adipocyte-containing cores and non-adipocytecontaining cores, which was expected as neither is a known LXR target gene and thus serves as an internal negative control. No significant association was found between TMA samples with adipocyte presence and survival outcome (P = 0.1303) (SFig. 3A).

To validate this finding in additional datasets, we performed the literature review and identified a publicly available dataset (GSE78958 (Toro *et al.* 2016)) that contained basal-like cancers (n = 98), which were annotated with categorical BMI data (<25, 25–29.99, 30+) and reported expression of LXR target gene ABCB1/Pgp. *ABCB1* mRNA expression was positively correlated with NR1H3/LXR α (r = 0.46, P = 0.0031), but interestingly, only in obese patients (Fig. 3B). Notably, this correlation was not found in Luminal A or Luminal B subtypes from the same dataset (SFig. 4). NR1H2/LXR β was positively correlated with ABCB1 only in normal-weight and overweight TNBC patients (r = 0.41, P = 0.0112; r = 0.3, P-0.0418 respectively) (Fig. 3B) and with ABCA1

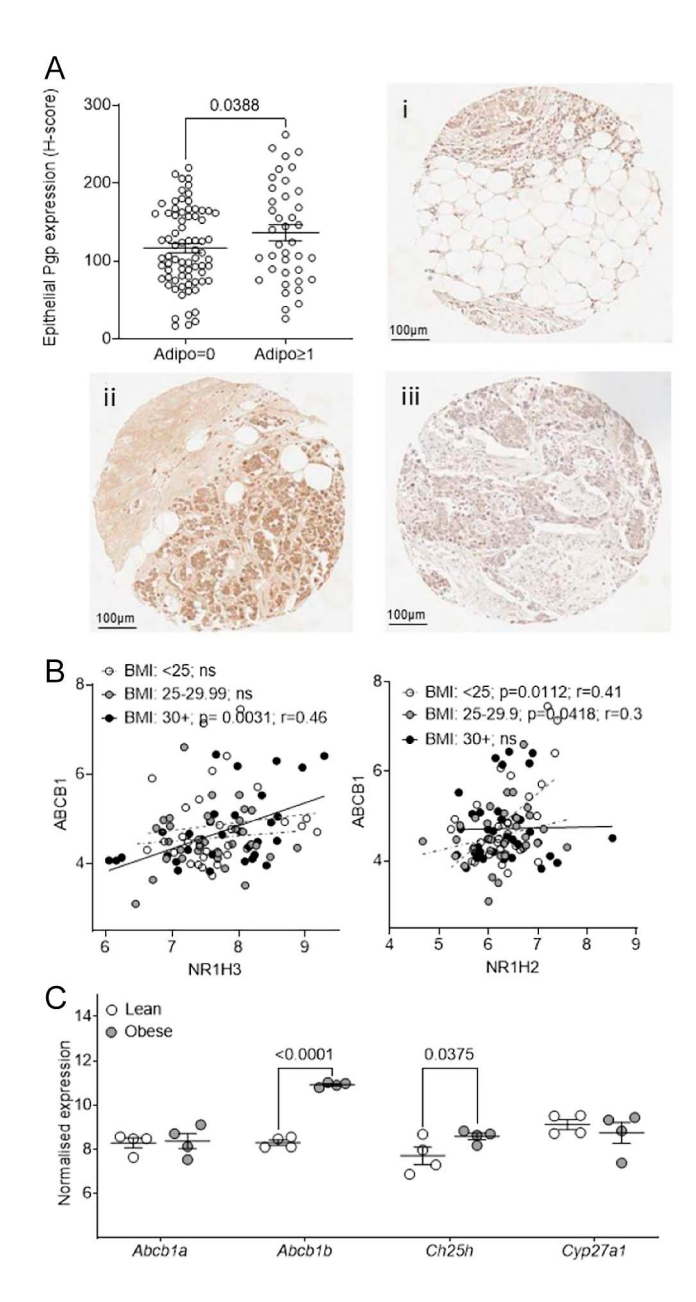


Figure 3

Obesity is associated with activity of the LXR: Pgp axis in TNBC patients and animal models. Presence of adipocytes is associated with elevated protein expression of Pgp (A) in a 148 TNBC patient tissue microarray. TMA samples are categorised as with or without adipocytes according to presence or absence of adipose cells in respective triplicate cores. Data shown are mean with SEM of samples with (n = 39) or without (n = 74)adipocytes with available Pgp staining, and analysed using unpaired parametric one-tailed t-test, in obese but not overweight or normalweight TNBC patients (GSE78958), Pgp is significantly positively correlated with NR1H3 (B), data shown are from patients with basal-like breast cancer (n = 98), and grouped according to BMI information (<25: n = 30; 25–29.99: n = 34; ≥30: n = 34), and analysed using one-tailed Spearman correlation. Gene expression (GSE151866) of Pap and Ch25h is elevated in TNBC tumours from obese mice compared to lean mice (C). Data shown are mean with SEM from obese (n = 4) and lean (n = 4) TNBC mice, and analysed using one-tailed unpaired t-test.

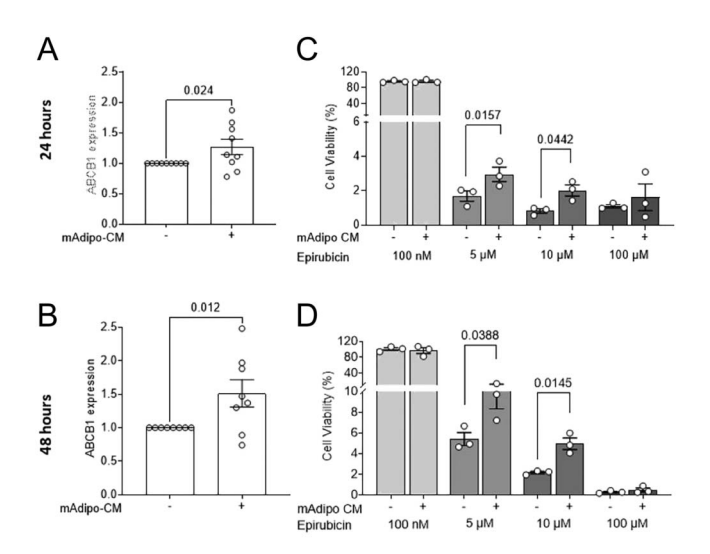


Figure 4

Adipocyte-conditioned confers resistance to epirubicin. Induction of ABCA1 and ABCB1 after culture with mAdipo-CM for 24 h (A) and 48 h (B). Data show mean of 7–9 independent replicates with standard error. One-tailed t-tests were used to compare means. mAdipo-CM confers resistance to epirubicin after 24 h (C) and 48 h (D). Data are normalised to matched 0% conditioned media. Data show mean with SEM of three independent replicates with standard error. One-tailed *t*-tests were used to compare means.

in overweight Luminal A or Luminal B patients (r = 0.24, P = 0.0205) (SFig. 4). Given the lack of Her2+ samples in the GSE78958 dataset, the analysis on this subtype was not performed. In addition, we identified a publicly available transcriptomic dataset from dietinduced obese mice implanted with the Py230 cell line model of basal-like breast cancer (GSE151866). In the Py230 tumours of the obese mice, there were significantly higher levels of Abcb1b (P < 0.0001) and Ch25h (P = 0.036) compared to the tumours of lean mice (Fig. 3C).

Adipocytes induce Pgp expression and confer chemoresistance in TNBC cells

Next, to determine if adipocytes could cause induction of Pgp in TNBC cells, mAdipo-CM was again harvested and added to MDA.MB.468 culture media. Culture of MDA.MB.468 cells with mAdipo-CM led to significant induction of ABCB1 gene expression (Fig. 4A and B; 24 h: 1.5-fold, P = 0.012; 48 h: 1.3-fold, P = 0.024) and enhanced survival in the presence of cytotoxic doses of epirubicin (Fig. 4C and D; P < 0.05). These data are consistent with the hypothesis that an adipocytesecreted factor(s) drives expression of the Pgp drug pump in cancer cells chemoresistance.

Discussion

The aim of this study was to test the hypothesis that the cholesterol store within adipocytes that are proximal to breast tumour tissue could provide a source of oxysterols that confer chemoresistance in TNBC. In vitro, adipocytes were found to contain and secrete relatively high levels of oxysterols, and when TNBC cancer cells were cultured with adipocyte-conditioned media, they increased expression of the LXR target gene Pgp and had greater resistance to epirubicin. In patients, the expression of several oxysterol-synthesising enzymes within the nontumour component of the tumour microenvironment was associated with elevated Pgp expression in the cancer cells and shorter DFS for the patients. The amount of adipose cells present in the TME of our TNBC cohort was also significantly associated with expression of CH25H, which is not just responsible for synthesising the LXR ligand 250HC, but is itself an LXRa target (Liu et al. 2018). Ch25h gene expression was elevated in the tumours of obese mice relative to lean, as was Abcb1/Pgp. We were unable to determine if CH25H expression was correlated with Pgp because it is synthesising the necessary ligand for LXR-driven transcription of the Pgp gene or because CH25H and Pgp are both under similar regulatory mechanisms; these are not mutually exclusive scenarios.

Notably, Pgp-mediated drug resistance has also been described in other tumour types, including leukaemia and brain cancers, where its expression has been associated with reduced therapeutic efficacy and poorer patient outcomes (Chan et al. 1991, Zhou et al. 1995, Legrand et al. 1999, Wang et al. 2017). This underscores the broader relevance of our findings, suggesting that the mechanisms we describe, particularly the induction of Pgp through metabolic cues such as oxysterols, may represent a conserved chemoresistance pathway.

In addition, 250HC and 270HC have molecular targets beyond LXRa that may contribute to our observations. 270HC was the most abundant oxysterol detected in our study, as has been reported previously (Solheim et al. 2019). This is notable given its emerging role in modulating tumour biology beyond its function as an LXR agonist. 270HC can interact with ERB, which is expressed in some TNBCs and can promote a feature also associated invasiveness, with chemoresistance (Mashat et al. 2022). 270HC also induces pro-survival signalling pathways such as IGF and EGF in TNBC cells, suggesting chemoresistance may be conferred through growth factor receptor modulation. 270HC's ability to induce changes in the immune cell complement of the TME in breast cancer (Baek et al. 2017) suggests another route by which chemoresistance may conferred be in physiologically representative breast cancer TMEs than was possible in our co-culture model. 250HC interacts with proteins such as SREBP2, ROR, GPR183 and several integrins (Odnoshivkina et al. 2022), which suggests 250HC can also modulate the local immune environment within the TNBC TME, thus leading to differential response to chemotherapy.

In previous work, ER-negative breast cancer was found to be more responsive to oxysterols and LXR signalling than ER-positive disease (Hutchinson et al. 2019), despite similar oxysterol concentrations between breast cancer subtypes (Solheim et al. 2019). Furthermore, activity of the LXR-Pgp axis in TNBC is linked to chemotherapy resistance and reduced patient survival (Hutchinson et al. 2021). If the OHC-LXR axis contributes to chemoresistance, attempts to reduce circulating cholesterol before commencing chemotherapy may dampen this resistance mechanism. However, this needs careful evaluation in the clinical trial setting. It is important to note that our data do not suggest that overweight/obesity per se exacerbates chemoresistance, but that conversion of cholesterol to oxysterols can occur independently of BMI. The proximity and abundance of adipose tissue in the breast cancer TME, coupled with TNBC being highly responsive to oxysterol signalling, may mean that sufficient oxysterols to contribute to chemoresistance are present in most triple-negative breast tumours and thus represent an innate, yet potentially modifiable, form of resistance. Interventions that decouple the cholesterol-oxysterol pathway, rather than just weight loss or cholesterol lowering, at least in the period between diagnosis and onset of neoadjuvant or adjuvant chemotherapy, may be most effective.

Our work has several important limitations. First, the induction of *Pgp* gene expression observed after culture with conditioned media was low to moderate, which, although common for modulation of this efflux pump by nutritional or metabolic factors (Hutchinson et al. 2021), may not be sufficient to explain the chemoprotection we observed, and other drug resistance pathways may have been induced. Although this induction was moderate, in the in vivo context, the local tumour cells are exposed for longer and to higher levels of oxysterols than we observed in conditioned media experiments. This could also mean that there are additional cell types contributing to the oxysterol pools in primary tumours that we have not recapitulated in our model. Although we found adipocytes to produce more oxysterols than CAFs, this is in the context of a single immortalised (albeit derived from a primary breast tumour) cell line, and we did not attempt to confirm these findings in the primary setting. Our comparisons of enzyme expression may therefore not be reproducible with other adipocyte or CAF sources, including analyses in primary material. These limitations should be addressed in future work because CAFs are able to confer chemoresistance in claudin-low (the work showed here is conducted exclusively in claudin-high TNBC cell lines) in an IFN-β-dependent manner (Broad et al. 2021), and there is extensive

cross-talk reported between LXR and IFN pathways in several tissue types (Hao *et al.* 2009, Reboldi *et al.* 2014, Miao *et al.* 2016).

Supplementary materials

This is linked to the online version of the paper at https://doi.org/10.1530/REM-25-0006.

Declaration of interest

The authors declare that there is no conflict of interest that could be perceived as prejudicing the impartiality of the work reported.

Funding

JLT and GC were supported by grants from Breast Cancer Research Action Group (3T57/9R17-02), and World Cancer Research Fund and World Cancer Research Fund International (IIG_FULL_2021_019). JLT and AW were supported by a grant from Breast Cancer UK (1803609) and scholarship funding from the School of Food Science and Nutrition, University of Leeds.

Data availability

Data supporting the findings of this study are available from the corresponding authors upon reasonable request.

Author contribution statement

JLT sourced funding for salaries and consumables. JLT and GC wrote the manuscript. GC and AW performed the laboratory experiments. LW built and counter-scored the TMA for IHC. AW and BW scored the TMA IHC. GC and YAH performed the adipocyte counts. HRL and AW performed oxysterol analysis. JLT, TAH and BK supervised the project. All authors approved the final manuscript.

Acknowledgements

CHUB-S7 pre-adipocytes were kindly provided by Dr Christian Darimont from Nestlé Research Centre under a Material Transfer Agreement signed 18-10-2019.

References

Baek AE, Yu Y-RA, He S, *et al.* 2017 The cholesterol metabolite 27 hydroxycholesterol facilitates breast cancer metastasis through its actions on immune cells. *Nat Commun* **8** 864.

(https://doi.org/10.1038/s41467-017-00910-z)

Bousquenaud MD I & Rüegg C 2022 Tumor genes regulated in obesity-mediated breast cancer. In *NCBI, Gene Expression Omnibus*. Ed SIO Bioinformatics. GEO (Gene Expression Omnbus).

(https://www.ncbi.nlm.nih.gov/geo/query/acc.cgi?acc=GSE151866)

Broad RV, Jones SJ, Teske MC, *et al.* 2021 Inhibition of interferon-signalling halts cancer-associated fibroblast-dependent protection of breast cancer cells from chemotherapy. *Br J Cancer* **124** 1110–1120.

(https://doi.org/10.1038/s41416-020-01226-4)

Chan HS, Haddad G, Thorner PS, *et al.* 1991 P-glycoprotein expression as a predictor of the outcome of therapy for neuroblastoma. *N Engl J Med* **325** 1608–1614. (https://doi.org/10.1056/nejm199112053252304)

Darimont C, Zbinden I, Avanti O, et al. 2003 Reconstitution of telomerase activity combined with HPV-E7 expression allow human preadipocytes to

preserve their differentiation capacity after immortalization. *Cell Death Differ* **10** 1025–1031. (https://doi.org/10.1038/sj.cdd.4401273)

Darimont C, Avanti O, Zbinden I, *et al.* 2006 Liver X receptor preferentially activates de novo lipogenesis in human preadipocytes. *Biochimie* **88** 309–318. (https://doi.org/10.1016/j.biochi.2005.08.010)

Decker NS, Johnson T, Vey JA, et al. 2023 Circulating oxysterols and prognosis among women with a breast cancer diagnosis: results from the MARIE patient cohort. BMC Med 21 438.

(https://doi.org/10.1186/s12916-023-03152-7)

Dent R, Trudeau M, Pritchard KI, *et al.* 2007 Triple-negative breast cancer: clinical features and patterns of recurrence. *Clin Cancer Res* **13** 4429–4434. (https://doi.org/10.1158/1078-0432.ccr-06-3045)

Hao XR, Cao DL, Hu YW, $et\,al.$ 2009 IFN-y down-regulates ABCA1 expression by inhibiting LXR α in a JAK/STAT signaling pathway-dependent manner. Atherosclerosis 203 417–428.

(https://doi.org/10.1016/j.atherosclerosis.2008.07.029)

Harborg S, Zachariae R, Olsen J, *et al.* 2021 Overweight and prognosis in triple-negative breast cancer patients: a systematic review and meta-analysis. *NPJ Breast Cancer* **7** 119.

(https://doi.org/10.1038/s41523-021-00325-6)

Hutchinson SA, Lianto P, Roberg-Larsen H, *et al.* 2019 ER-Negative breast cancer is highly responsive to cholesterol metabolite signalling. *Nutrients* **11** 2618. (https://doi.org/10.3390/nu11112618)

Hutchinson SA, Websdale A, Cioccoloni G, *et al.* 2021 Liver x receptor alpha drives chemoresistance in response to side-chain hydroxycholesterols in triple negative breast cancer. *Oncogene* **40** 2872–2883.

(https://doi.org/10.1038/s41388-021-01720-w)

Janowski BA, Willy PJ, Devi TR, *et al.* 1996 An oxysterol signalling pathway mediated by the nuclear receptor LXRo. *Nature* **383** 728–731. (https://doi.org/10.1038/383728a0)

Janowski BA, Grogan MJ, Jones SA, *et al.* 1999 Structural requirements of ligands for the oxysterol liver X receptors LXRα and LXRβ. *Proc Natl Acad Sci U S A* **96** 266–271. (https://doi.org/10.1073/pnas.96.1.266)

Kømurcu KS, Wilhelmsen I, Thorne JL, *et al.* 2023 Mass spectrometry reveals that oxysterols are secreted from non-alcoholic fatty liver disease induced organoids. *J Steroid Biochem Mol Biol* **232** 106355.

(https://doi.org/10.1016/j.jsbmb.2023.106355)

Kramer CJH, Vangangelt KMH, Van Pelt GW, et al. 2019 The prognostic value of tumour-stroma ratio in primary breast cancer with special attention to triple-negative tumours: a review. *Breast Cancer Res Treat* **173** 55–64. (https://doi.org/10.1007/s10549-018-4987-4)

Krause BR & Hartman AD 1984 Adipose tissue and cholesterol metabolism. J Lipid Res 25 97–110. (https://doi.org/10.1016/s0022-2275(20)37830-5)

Legrand O, Simonin G, Beauchamp-Nicoud A, *et al.* 1999 Simultaneous activity of MRP1 and Pgp is correlated with in vitro resistance to daunorubicin and with in vivo resistance in adult acute myeloid leukemia. *Blood* **94** 1046–1056.

(https://doi.org/10.1182/blood.v94.3.1046.415k03_1046_1056)

Lianto P, Hutchinson SA, Moore JB, et al. 2021 Characterization and prognostic value of LXR splice variants in triple-negative breast cancer. iScience 24 103212. (https://doi.org/10.1016/j.isci.2021.103212)

Liedtke C, Mazouni C, Hess KR, *et al.* 2008 Response to neoadjuvant therapy and long-term survival in patients with triple-negative breast cancer. *J Clin Oncol* **26** 1275–1281. (https://doi.org/10.1200/jco.2007.14.4147)

Liu Y, Wei Z, Ma X, *et al.* 2018 25-Hydroxycholesterol activates the expression of cholesterol 25-hydroxylase in an LXR-dependent mechanism. *J Lipid Res* **59** 439–451. (https://doi.org/10.1194/jlr.m080440)

Mashat RM, Zielinska HA, Holly JMP, et al. 2022 A role for ER-Beta in the effects of low-density lipoprotein cholesterol and 27-

Hydroxycholesterol on breast cancer progression: involvement of the IGF signalling pathway? *Cells* **11** 94.

(https://doi.org/10.3390/cells11010094)

Mcgraw KO & Wong SP 1996 Forming inferences about some intraclass correlation coefficients. *Psychol Methods* **1** 30–46.

(https://doi.org/10.1037//1082-989x.1.1.30)

Miao CM, He K, Li PZ, et al. 2016 LXRQ represses LPS-induced inflammatory responses by competing with IRF3 for GRIP1 in Kupffer cells. *Int Immunopharmacol* **35** 272–279.

(https://doi.org/10.1016/j.intimp.2016.04.009)

Millar EK, Browne LH, Beretov J, et al. 2020 Tumour stroma ratio assessment using digital image analysis predicts survival in triple negative and luminal breast cancer. Cancers 12 3749. (https://doi.org/10.3390/cancers12123749)

Odnoshivkina UG, Kuznetsova EA & Petrov AM 2022 25-Hydroxycholesterol as a signaling molecule of the nervous system. *Biochemistry* **87** 524–537. (https://doi.org/10.1134/s0006297922060049)

Reboldi A, Dang EV, Mcdonald JG, *et al.* 2014 Inflammation. 25-Hydroxycholesterol suppresses interleukin-1-driven inflammation downstream of type I interferon. *Science* **345** 679–684. (https://doi.org/10.1126/science.1254790)

Roberg-Larsen H, Lund K, Vehus T, *et al.* 2014 Highly automated nano-LC/MS-based approach for thousand cell-scale quantification of side chain-hydroxylated oxysterols. *J Lipid Res* **55** 1531–1536. (https://doi.org/10.1194/ilr.d048801)

Roberg-Larsen H, Lund K, Seterdal KE, et al. 2017 Mass spectrometric detection of 27-hydroxycholesterol in breast cancer exosomes. *J Steroid Biochem Mol Biol* **169** 22–28. (https://doi.org/10.1016/j.jsbmb.2016.02.006)

Rodrigues Dos Santos C, Fonseca I, Dias S, et al. 2014 Plasma level of LDL-cholesterol at diagnosis is a predictor factor of breast tumor progression. *BMC Cancer* **14** 132. (https://doi.org/10.1186/1471-2407-14-132)

Schmid P, Adams S, Rugo HS, *et al.* 2018 Atezolizumab and nab-paclitaxel in advanced triple-negative breast cancer. *N Engl J Med* **379** 2108–2121. (https://doi.org/10.1056/neimoa1809615)

Schmid P, Cortes J, Pusztai L, *et al.* 2020 Pembrolizumab for early triple-negative breast cancer. *N Engl J Med* **382** 810–821. (https://doi.org/10.1056/nejmoa1910549)

Shrout PE & Fleiss JL 1979 Intraclass correlations: uses in assessing rater reliability. *Psychol Bull* **86** 420–428.

(https://doi.org/10.1037//0033-2909.86.2.420)

Slenter DN, Kutmon M, Hanspers K, *et al.* 2018 WikiPathways: a multifaceted pathway database bridging metabolomics to other omics research. *Nucleic Acids Res* **46** D661–D667. (https://doi.org/10.1093/nar/gkx1064)

Solheim S, Hutchinson SA, Lundanes E, et al. 2019 Fast liquid chromatography-mass spectrometry reveals side chain oxysterol heterogeneity in breast cancer tumour samples. J Steroid Biochem Mol Biol 192 105309.

(https://doi.org/10.1016/j.jsbmb.2019.02.004)

Toro AL, Costantino NS, Shriver CD, et al. 2016 Effect of obesity on molecular characteristics of invasive breast tumors: gene expression analysis in a large cohort of female patients. BMC Obes 3 22.

(https://doi.org/10.1186/s40608-016-0103-7)

Verghese ET, Drury R, Green CA, *et al.* 2013 MiR-26b is down-regulated in carcinoma-associated fibroblasts from ER-positive breast cancers leading to enhanced cell migration and invasion. *J Pathol* **231** 388–399. (https://doi.org/10.1002/path.4248)

Wang N, Zhang Q, Ning B, et al. 2017 β -Asarone promotes Temozolomide's entry into glioma cells and decreases the expression of P-glycoprotein and MDR1. *Biomed Pharmacother* **90** 368–374.

(https://doi.org/10.1016/j.biopha.2017.03.083)

Zhou D, Zittoun R & Marie J 1995 Expression of multidrug resistance-associated protein (MRP) and multidrug resistance (MDR1) genes in acute myeloid leukemia. *Leukemia* **9** 1661–1666.